J. Mol. Biol. (1996) **258**, 661–671

JMB

Crystal Structure of the Pertussis Toxin–ATP Complex: A Molecular Sensor

Bart Hazes[1], Amechand Boodhoo[1], Stephen A. Cockle[2] and Randy J. Read[1]*

[1]*Department of Medical Microbiology and Immunology, University of Alberta, 1-41 Medical Sciences Building, Edmonton Alberta, T6G 2H7, Canada*

[2]*Connaught Centre for Biotechnology Research, 1755 Steeles Avenue West Willowdale, Ontario M2R 3T4, Canada*

**Corresponding author*

Pertussis toxin is a major virulence factor of *Bordetella pertussis*, the causative agent of whooping cough. The protein is a hexamer containing a catalytic subunit (S1) that is tightly associated with a pentameric cell-binding component (B-oligomer). *In vitro* experiments have shown that ATP and a number of detergents and phospholipids assist in activating the holotoxin by destabilizing the interaction between S1 and the B-oligomer. Similar processes may play a role in the activation of pertussis toxin *in vivo*. In this paper we present the crystal structure of the pertussis toxin–ATP complex and discuss the structural basis for the ATP-induced activation. In addition, we propose a physiological role for the ATP effect in the process by which the toxin enters the cytoplasm of eukaryotic cells. The key features of this proposal are that ATP binding signals the arrival of the toxin in the endoplasmic reticulum and, at the same time, triggers dissociation of the holotoxin prior to membrane translocation.

Keywords: pertussis toxin; endoplasmic reticulum; ATP binding; crystal structure; retrograde transport

Introduction

Whooping cough is a respiratory disease that still claimed over 300,000 lives in 1990, mostly children in developing countries (Galazka, 1992). In the developed countries morbidity has largely been controlled by vaccination, but the killed whole-cell vaccines have been under pressure after reports of side effects of varying severity (Howson *et al*., 1991). Consequently, many new vaccine formulations based on one or more purified bacterial antigens have been developed (Mortimer, 1994). Pertussis toxin (PT) has been a component of most acellular vaccines developed so far since it induces a strong protective immunity (Munoz *et al*., 1981a).

PT exerts its toxic activity inside eukaryotic cells by ADP-ribosylating the α-subunit of regulatory trimeric G-proteins ($G_{i\alpha}$) (Katada & Ui, 1982a). This prevents $G_{i\alpha}$ from inhibiting adenylate cyclase and consequently leads to an increase in the intracellular levels of cyclic AMP. Depending on the cell type that is affected, this can lead to numerous clinical symptoms including lymphocytosis, histamine sensitization and islet activation (Munoz *et al*., 1981b).

Before PT can reach its substrate $G_{i\alpha}$, the toxin has to cross the cell membrane to enter the cytoplasm. For this purpose PT is structurally organized into two distinct components, a catalytic subunit (S1) and a cell-binding pentamer (B-oligomer). The B-oligomer is composed of four types of subunits (S2, S3, two copies of S4, and S5) and binds to glycoconjugate receptors, preferably those bearing terminal sialic acid residues (Armstrong *et al*., 1988; Brennan *et al*., 1988). Crystallographic studies have identified equivalent sialic acid-binding sites in the S2 and S3 subunits (Stein *et al*., 1994a). After binding to cell-surface receptors the toxin is believed to enter the cell by endocytosis followed by intracellular trafficking to the compartment where membrane translocation takes place (Xu & Barbieri, 1995).

Several other bacterial and plant toxins that act in the cytosol of eukaryotic cells have been found to contain structurally distinct toxic (A) and cell-binding (B) domains. These toxins are generally referred to as the AB-toxins (Gill, 1978) and well-studied examples are PT, *Escherichia coli* heat-labile enterotoxin, cholera toxin, ricin, Shiga toxin, *Pseudomonas*

Abbreviations used: PT, pertussis toxin; CHAPS, 3-[(3-cholamidopropyl)dimethylammonio]-1-propanesulfonate; ER, endoplasmic reticulum; BFA, brefeldin A; PDI, protein disulphide-isomerase; rms, root-mean-square; CT, cholera toxin; LT, heat-labile enterotoxin; DT, diphtheria toxin.

0022–2836/96/190661–11 $18.00/0

exotoxin A and diphtheria toxin. A common characteristic of AB-toxins is that they all bind to the cell surface by means of their B component and enter the cell by endocytosis. Once in the cell there appear to be at least two distinct routes that lead to membrane translocation. Diphtheria toxin is transported to acidic endosomes where membrane translocation is triggered by the low pH (Moskaug *et al*., 1991). The route taken by the other toxins is less clear but is believed to involve the Golgi apparatus and possibly the endoplasmic reticulum (ER) (Pelham *et al*., 1992; Sandvig & van Deurs, 1994).

In 1982 it was demonstrated that PT is an ADP-ribosyltransferase (Katada & Ui, 1982b). In the same paper the authors showed that NAD and ATP were required to observe the ADP-ribosylation reaction in a washed membrane preparation of C6 glioma cells. NAD is the actual ADP-ribose donor in the reaction whereas the role of ATP was revealed through a series of subsequent studies. First of all, Moss *et al*. (1983) reported that the dependence on ATP was abolished in the presence of high concentrations of DTT, e.g. 250 mM for maximum activity. Since approximately 1 mM DTT is sufficient to activate a purified preparation of subunit S1 (Moss *et al*., 1986), it appears that constraints imposed by the interactions between subunit S1 and the B-oligomer are responsible for the resistance towards DTT-induced activation of the holotoxin. From further studies it became clear that the direct effect of ATP is to destabilize the interaction between the S1 subunit and the B-oligomer by binding to the B-oligomer (Moss *et al*., 1986; Hausman *et al*., 1990). The relaxation of the quaternary structure then indirectly activates the toxin by facilitating the subsequent reduction of a disulphide bond in the S1 subunit. It has been observed that CHAPS and several phospholipids also destabilize the interface between S1 and the B-oligomer, again leading to the activation of PT. However, only when both ATP and CHAPS are present together is actual dissociation of the S1 subunit observed (Burns & Manclark, 1986; Krueger & Barbieri, 1993).

Although the effects of ATP on PT activation have been studied in detail, little is known about its molecular basis. In addition, the physiological role of the ATP effect *in vivo* has not been established. We have determined the crystal structure of the PT–ATP complex at 2.7 Å resolution to address these questions, and to identify potential target residues for mutagenesis experiments.

Results

Quality of the structure

The crystals used in this study contain two holotoxin molecules per asymmetric unit, as described for the uncomplexed structure (Stein *et al*., 1994b). After superimposing the two molecules the root-mean-square (rms) deviation between all corresponding non-hydrogen atoms is 0.27 Å (maximum deviation is 0.69 Å). No strong indications for local deviations of non-crystallographic symmetry were noted. However, the *B*-values for subunits S1 and S5 in the two holotoxin molecules differ considerably. A similar situation exists in the native structure (see Table 1) and is probably caused by the less extensive crystal contacts made by the molecule with the higher *B*-values. We will refer to the two molecules as molecules 1 and 2, with the holotoxin having the lower *B*-values denoted molecule 1. In view of the close structural similarity between the molecules we will restrict the analysis given below to molecule 1.

In the final model each holotoxin molecule contains 7259 protein atoms in 935 amino acid residues, and 1 ATP molecule. Seventeen residues (S1: 1, S1: 211 to 220, S2: 1-2, S3: 1 to 3, S5: 1) in each molecule were not included since their electron density was too weak to be interpreted. In total 41 water molecules were added, 25 to molecule 1 and 16 to molecule 2. The *R*-factor for all reflections between 2.7 and 8 Å is 23.2% and the model has good stereochemistry (rms deviations from ideal bond lengths and angles are 0.017 Å and 2.0°, respectively). An analysis of the stereochemistry with the program PROCHECK (Laskowski *et al*., 1993) indicated that the model geometry is better than expected for a 2.7 Å structure for all tested properties (not shown). A phi–psi plot showing the main-chain dihedral angles is given in Figure 1.

The ATP-binding site

The ATP-binding site and the conformation of the nucleotide could be unambiguously established in a difference electron density map based on $\{|F_{ATP}| - |F_{native}|\}$ amplitudes and phases from the native PT model (see Figure 2(a)). The ATP molecule is bound in the central pore of the B-oligomer and makes extensive interactions with the protein (Figures 2(b), 3 and 4). The adenine ring is deeply buried and is packed between the helices of

Table 1. Overall *B*-values for individual PT subunits (Å^2)

	ATP-complex[a]		Native structure[b]	
Subunit	PT1[c]	PT2[d]	PT1[c]	PT2[d]
S1	12.77	57.11	10.56	54.90
S2	13.41	18.69	13.77	18.92
S3	13.65	24.06	13.50	22.46
S4a	10.17	14.55	9.93	15.42
S4b	8.08	29.69	8.45	28.48
S5	17.14	45.33	17.49	42.94

[a] The presented results were obtained by *B*-value refinement of the final ATP–complex structure allowing one *B*-value per subunit.
[b] The presented results were obtained by *B*-value refinement of the native PT structure allowing one *B*-value per subunit (Stein *et al*., 1994b).
[c] The *B*-values for holotoxin molecule 1.
[d] The *B*-values for holotoxin molecule 2.

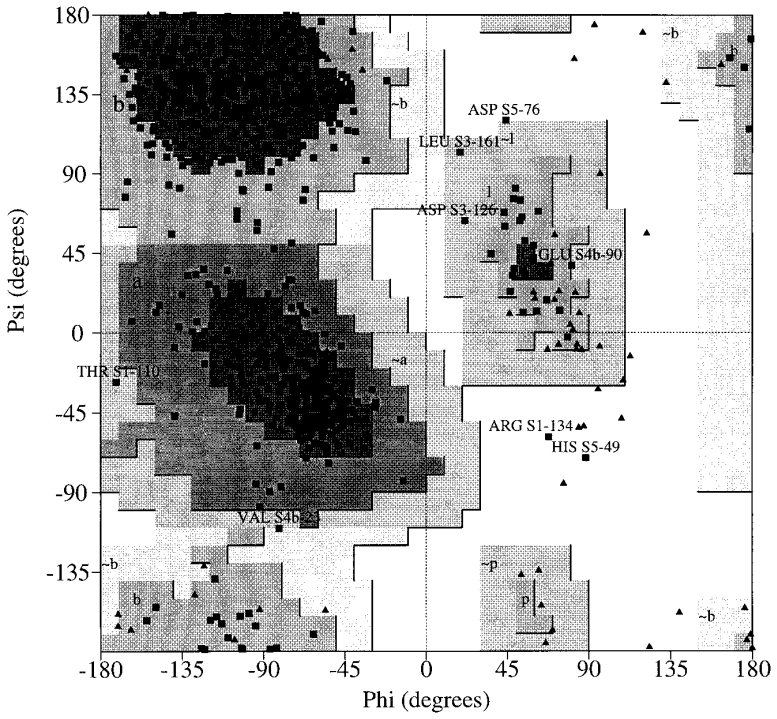

Figure 1. Phi–psi plot of PT molecule 1 in the final structure. Filled triangles and squares represent glycine and non-glycine residues, respectively. Residues with less favourable conformations are labelled. Arg S1-134 and His S5-49 have high energy conformations. His S5-49 is located in a surface-exposed loop and has relatively high *B*-values (38.8 Å^2, on average). The unfavourable phi–psi angles may therefore indicate a slight inaccuracy in the model, but the density does not suggest a clear alternative. Arg S1-134, in contrast, has normal *B*-values (21.7 Å^2, on average) and is located in a tight turn between two β-strands. Therefore, the strain in this residue may at least partly represent an actual structural constraint. This diagram was prepared by the program PROCHECK (Laskowski *et al*., 1993).

subunits S5 and S4b in a relatively spacious pocket (Figures 3 and 4). Its interactions with the protein are dominated by van der Waals contacts with the aliphatic portion of the side-chain of Arg S4b-69 and the aromatic ring of Phe S5-59 (see Figures 3(b) and 4(a)). Of the four nitrogen atoms in the adenine ring, only N-7 forms a hydrogen bond with the protein (Ser S5-62). The amine group at position 6 and the N-1 and N-3 nitrogen atoms do not have a protein-derived hydrogen bonding partner; how-

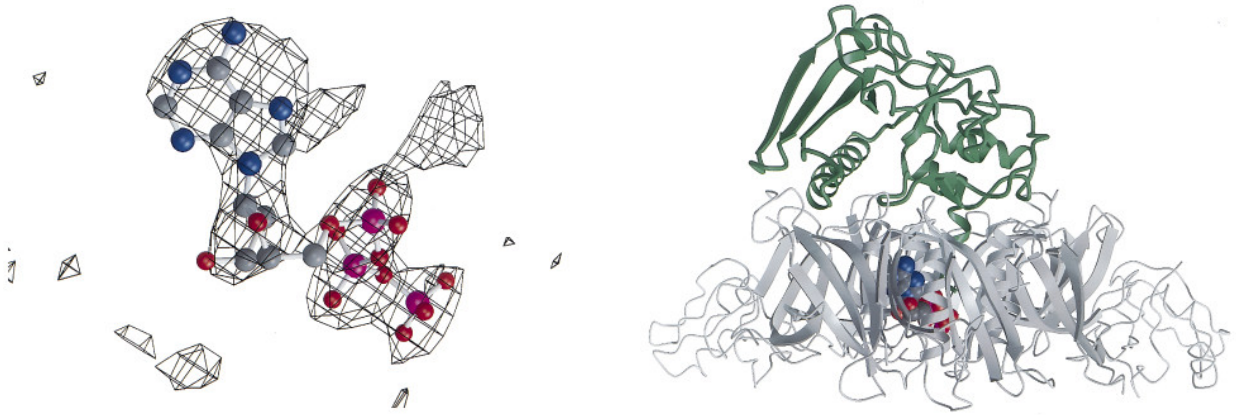

(a) **(b)**

Figure 2. (a) Electron density in the ATP-binding site contoured at a 3 sigma level. The electron density was calculated using observed amplitudes of the ATP-complex and native crystals and phase information from the native model ($\{|F_{ATP}| - |F_{native}|, \varphi_{native}\}$ coefficients). The model for ATP was taken from the refined structure of the complex. The additional density feature above and to the left of the α-phosphate indicates a side-chain reorientation of Arg69 in the S4b subunit, whereas the density feature above and to the right of the α-phosphate illustrates a shift of the C terminus of the S1 subunit upon ATP binding (see Figure 5). (b) C$^\alpha$ trace of the holotoxin–ATP complex in the same orientation as (a). The S1 subunit is shown in green, the B-oligomer in grey and the ATP molecule has been rendered as a CPK model with the carbon, nitrogen, phosphate and oxygen atoms coloured grey, blue, purple and red, respectively. The C terminus of the S1 subunit penetrates the central pore of the B-oligomer, and the terminal residue is just visible to the right of the triphosphate moiety of ATP. The secondary structural elements were assigned as reported by Stein *et al*. (1994b) except for the N-terminal domains of the S2 and S3 subunits, at the far right and left, respectively, which are depicted as coils. Panels (a) and (b) were rendered using MOLSCRIPT (Kraulis, 1991) and RASTER3D (Merritt & Murphy, 1994), whereas the density for (a) was created with the MINIMAGE program (Arnez, 1994).

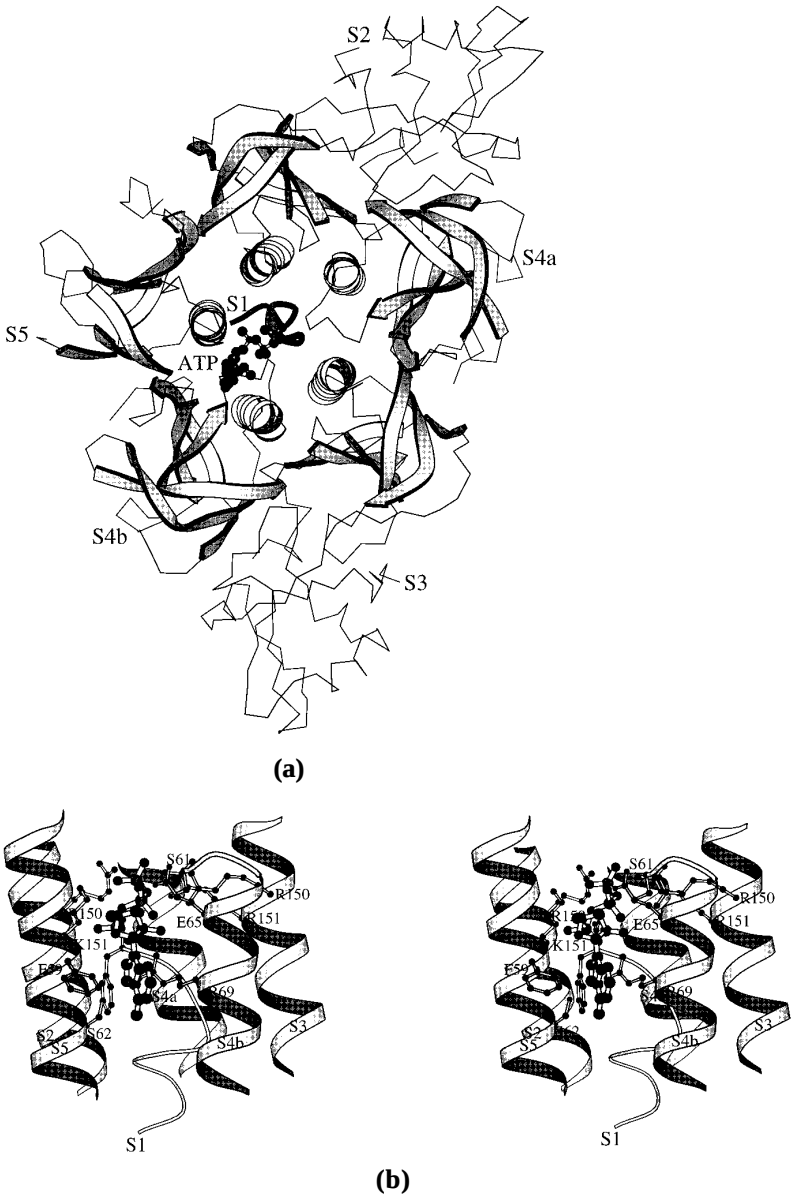

Figure 3. (a) Schematic diagram of the B-oligomer viewed along the central pore from the surface opposite to S1. The ATP molecule, in ball-and-stick representation, and the C terminus of the S1 subunit, shown as a coil, penetrate the central pore from opposite sides. Note that the adenine moiety is stacked in between the helices of subunits S4b and S5 whereas the triphosphate occupies a more central position. (b) Stereo figure of the ATP-binding site viewed perpendicular to the central pore. In this orientation, the main body of S1 is at the bottom and ATP enters the central pore from the top. The residues that dominate the protein–ATP interactions are drawn in ball-and-stick representation. These residues are labelled by their one-letter amino acid code and their residue number. Each helix is labelled with a subunit identifier. Panels (a) and (b) were rendered using the program MOLSCRIPT (Kraulis, 1991).

ever, at the current resolution we cannot exclude the possibility of solvent-mediated interactions with the protein. The ribose moiety is also in a buried position and its 2' and 3' hydroxyl groups are hydrogen-bonded to the side-chains of Ser S4b-61 and Glu S4b-65, respectively (Figure 4). The triphosphate moiety is partly exposed at the surface opposite to the S1 subunit, and five positively charged amino acids; *viz* Arg S2-150, Lys S2-151, Arg S3-150, Arg S3-151 and Arg S4b-69 provide favourable hydrogen bonding and electrostatic interactions (Figures 3 and 4). In contrast, the negatively charged carboxyl terminus of subunit S1 interacts unfavourably with the four negative charges of the triphosphate moiety, causing a displacement of the C-terminal three residues (see below). The presence of a glycine at position S5-58 appears to be essential to ATP binding. The orientation of the main-chain is such that any other residue at this position would cause a steric conflict between its C^{β} atom and a phosphate oxygen (Figure 4(a)). Since the phi–psi angles of glycine S5-58 fall in the normal α-helical region of the Ramachandran plot (–66°, –45°) mutation of this residue should be permissible.

The position and conformation of ATP bound to the two holotoxin molecules in the asymmetric unit are comparable, although no non-crystallographic symmetry restraints were applied on the ATP molecules during refinement. The average *B*-values for ATP in molecule 1 and 2 were 17.6 $Å^2$ and 25.8 $Å^2$, respectively.

Comparison with the native model

The overall quaternary and tertiary structure of the PT holotoxin does not change significantly upon ATP binding, and the native (Stein *et al*., 1994b) and ATP–complex structures can be superimposed with an rms deviation of 0.38 Å for all 934 corresponding

C^{α} atoms. A number of minor modifications, mostly in side-chain conformations, were made during refinement. This probably reflects the better quality of the diffraction data for the ATP–complex rather than true differences between the native and ATP–complex structures. Significant structural changes are only observed in the ATP-binding site, which is most clearly shown in Figure 5. Arginine S4b-69 has adopted a different side-chain conformation in the ATP–complex structure. This prevents a steric conflict with the adenine ring of ATP and results in favourable van der Waals interactions between the aliphatic portion of the side-chain and the plane of the adenine ring. Furthermore, it leads to a favourable interaction between the guanidinium group and the α-phosphate (see Figure 4). The second conformational change concerns the C terminus of the S1 subunit, which is moved away from the triphosphate moiety to reduce electrostatic repulsion and steric hindrance. This movement affects residues 233 to 235 in which the C^{α} atoms shift by 0.6, 1.0 and 1.3 Å, respectively (Figure 5). However, even after this conformational change the carboxyl oxygen atoms remain in close proximity to the phosphate oxygen atoms (Figure 4).

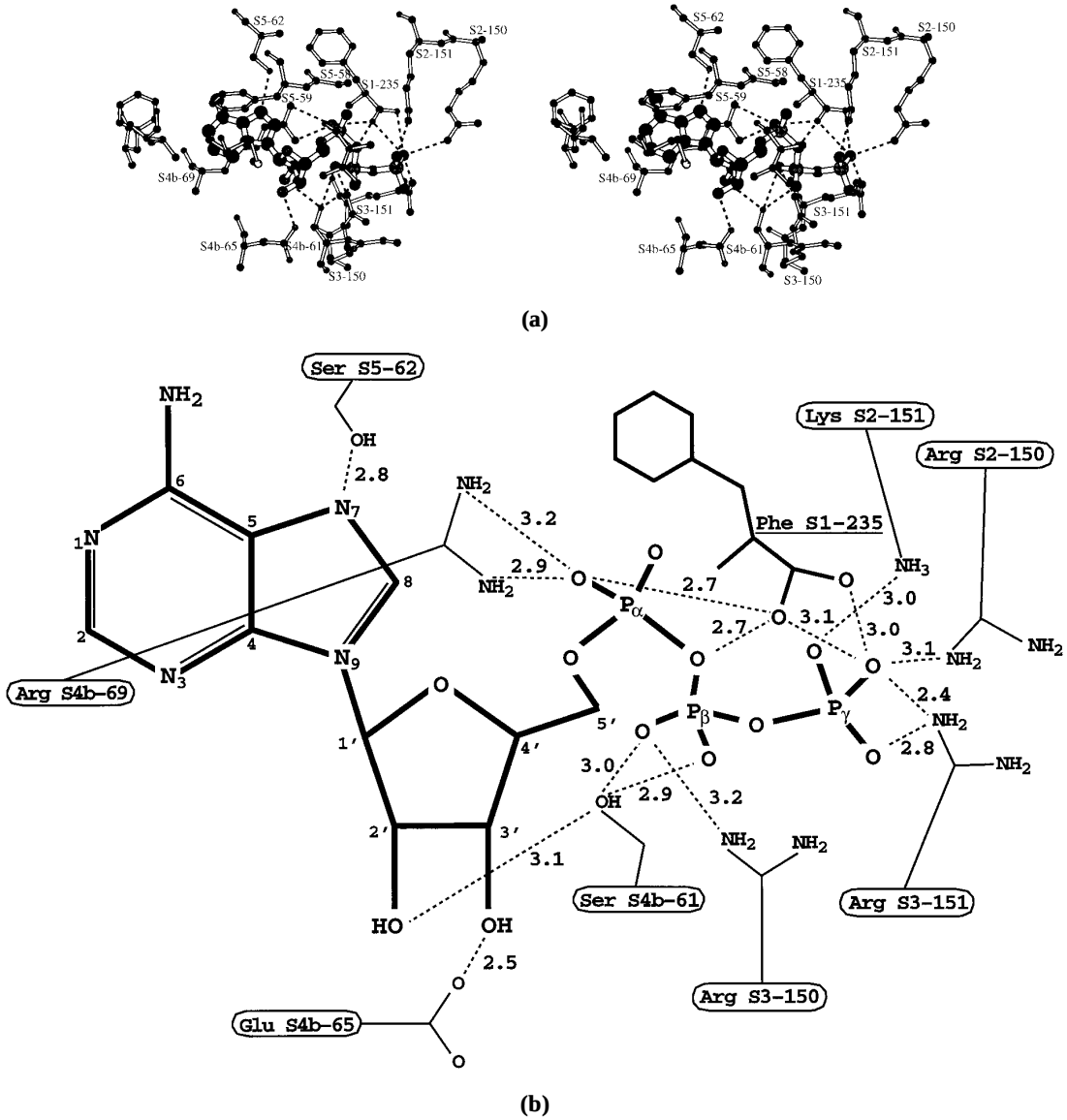

Figure 4. Details of the protein–ATP interactions. (a) Stereo figure showing the interactions between the protein and ATP. All residues that have at least one atom closer than 4.0 Å from any ATP atom are shown. Note that there is sufficient space to allow GTP binding (GTP has an additional substituent at the 2 position of the six-membered ring). Hydrogen bonds between the protein and ATP atoms are displayed as broken lines. Broken lines have also been used to indicate short contacts between the triphosphate oxygen atoms and the C terminus of subunit S1 although not all of them can actually form hydrogen bonds. (b) Schematic drawing of the hydrogen bonds between the protein and ATP. The orientation is comparable to (a).

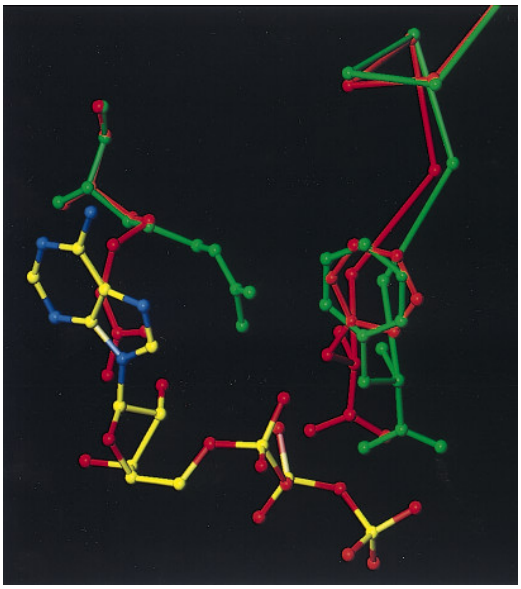

Figure 5. ATP-induced structural changes in the side-chain conformation of arginine 69 of the S4b subunit and the C terminus of subunit S1. The native structure is shown in red and the ATP–complex structure in green. The ATP-induced conformational changes can be recognized in a difference electron density map (see Figure 2(a)).

Discussion

In the structure of the PT–ATP complex we observe a single ATP-binding site in the central pore of the B-oligomer. This agrees with the work of Hausman *et al*. (1990) who reported that ATP binds to the B-oligomer and the holotoxin but not to the S1 subunit. The same authors determined the number of binding sites to be 0.2 for the holotoxin and 0.46 for the B-oligomer. The cause for this non-integral number of binding sites could not be established, but it was suggested that it might be due to an unidentified competitive inhibitor. Our structural results clearly indicate that there is exactly one binding site per B-oligomer which, based on the relatively low *B*-values, appears to be fully occupied in our experiments. It should, however, be noted that the crystals were soaked in 30 mM ATP, which is much higher than the micromolar ATP concentrations used in the reported binding studies.

Several studies have probed the affinity and specificity of the ATP-binding site (Lim *et al*., 1985; Burns & Manclark, 1986; Mattera *et al*., 1986; Moss *et al*., 1986; Kaslow *et al*., 1987; Hausman *et al*., 1990). Although there is considerable variation in the reported results all studies find that ATP binds most tightly, ADP binds with lower affinity and AMP shows no clear binding. This indicates that the triphosphate moiety contributes significantly to the binding energy which, according to the crystal structure, originates from the direct interaction between the triphosphate moiety and the five Arg/Lys residues on the B-oligomer (Figure 4). Another general observation is that GTP binds less tightly than ATP and that CTP and TTP binding is again weaker than GTP binding. This indicates that the binding site has a distinct specificity for adenine nucleotides. The lower affinity for GTP may be caused by the fact that guanine has two hydrophilic ring substituents, an amine at the 2 position and a carbonyl oxygen at the 6 position, whereas adenine only has a single amine group at the 6 position. Burying the additional hydrophilic group of guanine in the hydrophobic binding pocket could account for the reduced affinity.

An interesting phenomenon emerged in experiments carried out by Mattera *et al*. (1986). They showed that ATP and GTP, when added in saturating concentrations, are equally effective in activating PT. This indicates that the different substituents on the purine ring affect the binding affinity, but not the activation mechanism. In contrast, if GDP is added in saturating concentrations it remains less effective than ATP or GTP. This is consistent with the model that the electrostatic and steric repulsion between the triphosphate moiety and the C terminus of subunit S1 forms the mechanism by which the interaction between S1 and the B-oligomer is destabilized. The importance of the triphosphate moiety in the activation mechanism is further supported by the observation that triphosphate by itself can activate the toxin (Kaslow *et al*., 1987).

Mattera *et al*. (1986) demonstrated a lag phase in the activation of PT after the addition of nucleotides and substrates (up to 25 minutes when using GDP as the activator, less with ATP). The lag phase disappeared when the toxin was treated with GDP or ATP before addition of the substrates. A potential explanation for this behaviour is that nucleotide binding to PT is a kinetically slow process. The static nature of the crystal structure does not provide pertinent information on kinetic processes; however, it appears that the nucleotide can only enter the pore of the B-oligomer through a small opening on the side opposite to the S1 subunit. It is conceivable that this forms a significant kinetic barrier.

The position of the ATP-binding site also has implications for results reported by Hausman *et al*. (1990) on the relationship between ATP binding and the attachment of eukaryotic sialoglycoconjugates. In this study it was reported that whereas ATP had no effect on the haemagglutination of red blood cells by PT, the sialoglycoprotein fetuin significantly inhibited ATP binding to PT. The lack of reciprocity between the two binding events argues against overlapping binding sites (Hausman *et al*., 1990). The two equivalent sialic acid-binding sites identified by crystallography on the S2 and S3 subunits (Stein *et al*., 1994a), which are believed to represent the eukaryotic receptor sites, are both more than 40 Å away from the opening of the ATP-binding pocket. If there are no secondary receptor-binding sites on PT, then this indeed rules out overlapping ATP and receptor-binding sites. The buried position of ATP would also be difficult to

reconcile with overlapping binding sites. As an alternative explanation Hausman *et al*. (1990) suggested that fetuin binding might lower the affinity for ATP by triggering a conformational rearrangement of the B-oligomer. However, the structure of the PT–carbohydrate complex (Stein *et al*., 1994a) provides no evidence for such a conformational change. In addition, if an allosteric interaction were to exist between the ATP and receptor-binding sites, then one would still expect a reciprocal effect between ATP and receptor binding. The observations are more readily explained by assuming that fetuin binding further increases the kinetic barrier of ATP binding referred to in the paragraph above. It is plausible that binding of fetuin reduces the flexibility of the B-oligomer, particularly when both the binding sites on the S2 and S3 subunits are involved. This could increase the kinetic barrier to the degree that full occupation of the ATP-binding site is no longer attained in the time allotted to the experiment. Clearly, more work is required to fully understand the interplay between the ATP and receptor-binding sites.

As presented above, the crystal structure of the PT–ATP complex provides a structural basis for most of the biochemical properties that have been reported. However, the ultimate question regarding the physiological role of ATP binding *in vivo* has not been adequately addressed. In previous work, most hypotheses have focused on the activation of PT by cytosolic ATP (Burns & Manclark, 1986; Kaslow *et al*., 1987; Hausman *et al*., 1990). However, several observations suggest that the A and B domains of other AB-toxins already dissociate before or during translocation of the A domain into the cytosol. If that is the case with PT then the source of ATP, causing the S1/B-oligomer destabilization, has to be a pre-cytosolic compartment. To our knowledge the only compartment on the protein export pathway that is known to contain ATP is the endoplasmic reticulum (Braakman *et al*., 1992; Clairmont *et al*., 1991). Interestingly, the ER has also been implicated as the target compartment for a number of other AB-toxins, as outlined below.

Yoshida *et al*. (1991) showed that cells could be protected against ricin, modeccin and *Pseudomonas* exotoxin A (ExoA) by the fungal drug brefeldin A (BFA). BFA leads to the disruption of the Golgi apparatus, and consequently the involvement of the Golgi apparatus in the entry of these toxins into the cytoplasm was proposed. A similar protection of cells by BFA has been observed for PT (Xu & Barbieri, 1995), cholera toxin (CT) (Nambiar *et al*., 1993; Orlandi *et al*., 1993; Donta *et al*., 1993) and *Escherichia coli* heat-labile enterotoxin (LT) (Donta *et al*., 1993), suggesting that they share a common mechanism of cell entry. Indirect evidence that such toxins actually travel through the Golgi apparatus to the ER comes from the observation that CT, LT and ExoA have an ER-retention signal. The ER-retention signal, a C-terminal Lys-Asp-Glu-Leu (KDEL) or related tetrapeptide, is known to cause retrograde transport of proteins from the Golgi to the ER by means of a KDEL-receptor protein (Nilsson & Warren, 1994). The functional importance of the ER-retention signal is supported by the observation that the toxicity of ExoA decreases when its ER-retention signal is removed (Chaudhary *et al*., 1990), and conversely, ricin becomes more toxic upon addition of a KDEL sequence to its C terminus (Wales *et al*., 1992). For Shiga toxin the ability to enter the ER has actually been visualized by electron microscopy in A431 cells that were treated with butyrate (Sandvig *et al*., 1994). Based on these observations it has been postulated that the toxins mentioned above undergo retrograde transport from the plasma membrane *via* the Golgi apparatus to the ER, where finally membrane translocation takes place in an as yet unknown manner (Pelham *et al*., 1992; Sandvig & van Deurs, 1994).

The dissociation of the A and B domains of AB-toxins prior to membrane translocation has not been fully established. The most direct evidence for such a dissociation event comes from a study on ExoA in which the authors showed that only the A domain enters the cytosol (Ogata *et al*., 1990). The structural organization of AB-toxins is certainly consistent with a dissociation event occurring prior to translocation, as is shown schematically in Figure 6. All AB-toxins except PT appear to require both proteolytic cleavage of a peptide loop and reduction of a disulphide bond for expression of toxicity (Ogata *et al*., 1990; Gordon & Leppla, 1994; Grant *et al*., 1994; Freedman *et al*., 1994). Both processes are also necessary for dissociation of the A and B domains to occur. In several cases it has been shown that intracellular proteases are responsible for the proteolytic cleavage of AB-toxins (reviewed by Gordon & Leppla, 1994). Reduction of the disulphide bond in the oxidizing environment of the protein export pathway is also believed to require host factors. For diphtheria toxin (DT) this host factor has been shown to be a protein disulphide-isomerase (PDI) that is located on the cell surface (Mandel *et al*., 1993). For ExoA it was found that proteolytic cleavage occurs in an early endosomal compartment, whereas disulphide bond reduction occurs later and requires a functional ER-retention signal (Ogata *et al*., 1990). Based on the latter observation and the fact that PDIs are most abundant in the ER, it is conceivable that disulphide bond reduction of the AB-toxins that travel to the ER occurs preferentially in that compartment. Interestingly, an ExoA variant which has lost the disulphide bond by mutating the two cysteine residues to serine residues is still toxic *in vitro* but non-toxic *in vivo* (Madshus & Collier, 1989). One interpretation of this result is that a premature dissociation of the A and B domains, after proteolytic cleavage in the endosomes, prevents further trafficking of the A-domain to the ER.

In vitro activation of PT also requires reduction of a disulphide bond (Moss *et al*., 1983), though this is not directly connected with A-B dissociation. Cleavage of the single disulphide bond in subunit S1 (Cys41–Cys201) is believed to trigger a con-

formational change necessary to expose the active site to its substrates (Stein *et al*., 1994b). It is noteworthy that in the holotoxin, the S1 disulphide bond is very resistant to reduction in the absence of ATP (Moss *et al*., 1983), suggesting that *in vivo*, the reduction step takes place after interaction of PT with ATP. Reduction of the S1 disulphide bond also affects the interaction of PT with model membranes (Hausman & Burns, 1992). This could be relevant to the mechanism of membrane translocation, since the catalytic subunit at least appears to remain membrane associated after translocation into the cytosol (Xu & Barbieri, 1995). As pointed out (Stein *et al*., 1994b), the segment 184–203 of the S1 subunit, which should become more exposed on disulphide bond reduction, scores highly as a potential membrane-spanning helix.

Proteolytic cleavage of PT is not required for the expression of toxicity *in vitro*, but the potential involvement *in vivo* has not been established. Subunit S1 does contain a double basic site at Arg181–Arg182, which could be a target for furin-related host proteases (Gordon & Leppla, 1994). Although cleavage at this position preserves the catalytic site, loss of the C terminus adversely affects binding to the protein substrate $G_{i\alpha}$ (Krueger & Barbieri, 1994) and abolishes the interaction of S1 with model membranes (Hausman & Burns, 1992). However, *in vitro*, preferential cleavage of S1 in the holotoxin by trypsin and chymotrypsin has been reported at sites closer to the C terminus (Arg218 and Trp215). Cleavage in this region, which is a disordered loop in the crystal structure (Stein *et al*., 1994b), does not interfere with the ADP–ribosylation reaction and it leaves the putative membrane spanning segment intact. However, it does not by itself cause dissociation of the A and B domains (Krueger *et al*., 1991).

Conclusion

Current information suggests that dissociation of most AB-toxins occurs as a result of proteolytic cleavage and reduction of a disulphide bond. Proteolytic cleavage most likely occurs before entering the ER, whereas we suggest that disulphide bond reduction occurs preferentially in the ER where it can be mediated by PDIs. Although dissociation of PT is not required for catalytic activity, it is likely that dissociation must precede membrane translocation. We suggest that the central event leading to dissociation of S1 from the

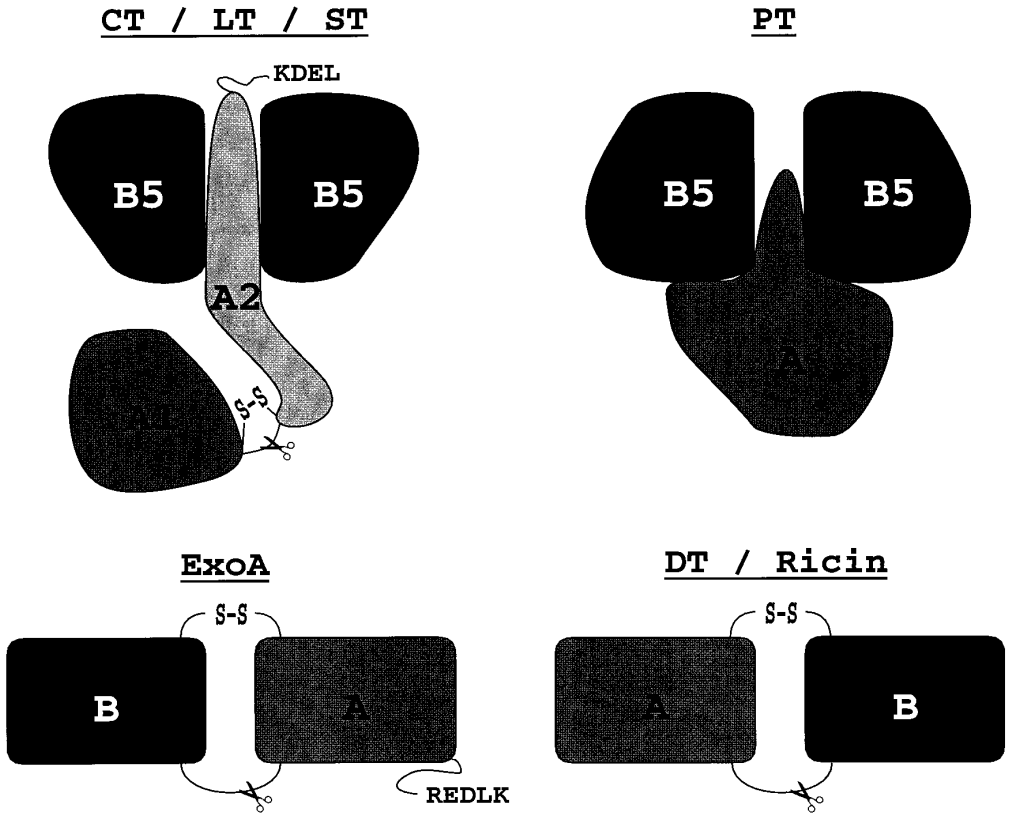

Figure 6. Schematic diagram showing the structural organization of several AB-toxins; *viz* cholera toxin (CT), *E. coli* heat-labile enterotoxin (LT), Shiga toxin (ST), pertussis toxin (PT), *Pseudomonas* exotoxin A (ExoA), diphtheria toxin (DT) and ricin. The catalytic component (A) is grey and the binding component (B) is black. The A domain of CT, LT and ST can be further divided into a N-terminal catalytic domain (A1) and a C-terminal domain (A2) that anchors domain A1 to the pentameric binding component. The ER-retention signal at the C terminus of the A2 domain is KDEL in CT, RDEL in LT and is absent in ST. The pair of scissors indicates the presence of a protease-sensitive loop. Disulphide bonds that link A and B domains are indicated as -S-S-.

B-oligomer is the binding of ATP to the B-oligomer in the ER. This may be facilitated by prior proteolytic cleavage, subsequent reduction of the S1 disulphide bond and / or binding of phospholipids. In this manner, the ATP-binding site would act both as a molecular sensor that detects the arrival in the ER, and as the trigger that initiates dissociation of the holotoxin prior to membrane translocation of the catalytic subunit.

Materials and Methods

PT crystals were obtained as described (Stein *et al*., 1994b) and had a typical size of 0.3 mm × 0.2 mm × 0.15 mm. The space group is $P2_12_12_1$ with cell parameters a = 163.8 Å, b = 98.2 Å and c = 194.5 Å. There are two holotoxin molecules per asymmetric unit referred to as molecule 1 and molecule 2. The crystal that was used for data collection was soaked for one day in mother liquor (25 mM sodium / potassium phosphate (pH 8.0), 0.25 M KCl, 0.02% (w / v) NaN_3) to which 30 mM ATP was added. Diffraction experiments were carried out at room temperature using synchrotron radiation (λ = 1 Å) from beamline $BL6A_2$ at the Photon Factory (Tsukuba, Japan). Data were recorded on Fuji image plates using the Weissenberg camera (Sakabe, 1991), integrated using the program WEIS (Higashi, 1989) and reduced with programs in the BIOMOL package (University of Groningen). A total of 195,544 reflections were reduced to 62,637 unique reflections to 2.5 Å resolution. The R_{sym} ($100 \times \Sigma|I - \langle I \rangle| / \Sigma\langle I \rangle$) for all symmetry-related reflections was 9.3%. Data completeness is 64.0% to 2.7 Å resolution with 19.6% completeness in the highest resolution shell. Data completeness falls off quickly with resolution due to radiation damage. This reduced the effective resolution from approximately 2.5 Å in the first exposure to 3.3 Å at the end of the data collection.

The ATP-soaked crystals were isomorphous with the crystals used for the native data set and, after applying an overall scale factor and an isotropic B-value, the R-factor (on amplitudes) between the two data sets was 15.4%. The native model was therefore directly used as the initial model for refinement, except that the individual B-values were reset to an overall B-value of 25 Å^2. Refinement was carried out with the program X-PLOR using standard protocols (Brünger, 1992a) and manual rebuilding was performed with the program O (Jones *et al*., 1991). Initial refinement consisted of rigid body refinement, treating each of the 12 subunits in the asymmetric unit as a rigid body, followed by a B-value refinement allowing one overall B-value per subunit. This reduced the R-factor from 31.1% to 28.4% (8 to 3 Å). At this stage $2mF_o - DF_c$ and $mF_o - DF_c$ SIGMAA weighted electron density maps (Read, 1986) were computed to check the model. In both maps a prominent density feature with the expected shape for an ATP molecule was observed and a molecular model for ATP (Cini & Marzilli, 1988) was modelled in this density. The side-chain of Arg 69 in the S4b subunit had to undergo a conformational change to allow ATP binding. Since no continuous side-chain density was present at this stage, this residue was temporarily modified to an alanine. The new model was further refined by energy minimization using non-crystallographic symmetry restraints between the two holotoxin molecules in the asymmetric unit. This reduced the R-factor to 25.5% (2.7 to 8 Å). In a subsequent model building session the side-chain of Arg69 could be reinserted into the model and numerous other minor improvements were made. Another energy minimization run followed by a restrained individual B-value refinement yielded a model with an R-factor of 23.8% (2.7 to 8 Å) which was used for further model building. In this session 81 water molecules were added to the model and an additional residue (Pro3 of the S2 subunit) could be added to both molecules in the asymmetric unit. Refinement was continued by simulated annealing after the individual B-values from the previous cycle were reset to their original values with one B-value per monomer. This reduced the R-factor to 22.6% (2.7 to 8 Å) and the resulting model was used for an extensive model building session. After rebuilding molecule 1 we discovered that the non-crystallographic symmetry restraints had not been switched on during the simulated annealing refinement. Since the manual modifications made to molecule l were based on density features that could not be the result of model bias we decided to keep molecule 1 and to restore ideal non-crystallographic symmetry by replacing molecule 2 by an appropriately positioned copy of molecule 1. A cycle of energy minimization and simulated annealing resulted in an R-value of 25.0% (2.7 to 8 Å) which was further reduced to 22.9% (2.7 to 8 Å) by a tightly restrained B-value refinement, using restraints of 0.25 and 0.5 for bonded main-chain and side-chain atoms, respectively. The validity of refining individual B-values at this resolution was checked by repeating the B-value refinement with 2240 reflections held apart for a free R-factor analysis. During this refinement the free R-factor (Brünger, 1992b) dropped from 24.2 to 22.8% indicating a true improvement of the model. In the last step 40 of the 81 water molecules were rejected from the model, retaining only well defined water molecules that occur in both non-crystallographically related molecules (6 in each molecule) or water molecules that make at least two hydrogen bonds to the protein (each shorter than 3.2 Å) and have B-values below 20 Å^2. This raised the R-factor slightly to 23.2% but we felt that a conservative placement of water molecules was more appropriate given the resolution of our data. The co-ordinates and structure factors of the PT–ATP complex have been deposited at the Protein Data Bank with accession code 1BCP and will be released one year after deposition.

Acknowledgements

We thank N. E. C. Duke, A. Nakagawa and N. Sakabe for help with data collection. This work was supported by grants to R.J.R. from the Medical Research Council of Canada (MRC) and the Alberta Heritage Foundation for Medical Research (AHFMR), and in part by an International Research Scholars award to R.J.R. from the Howard Hughes Medical Institute. B.H. acknowledges research allowances form the MRC, the AHFMR and the Izaak Walton Killam Trust.

References

Armstrong, G. D., Howard, L. A. & Peppler, M. S. (1988). Use of glycosyltransferases to restore pertussis toxin receptor activity to asialogalactofetuin. *J. Biol. Chem.* **263**, 8677–8684.

Arnez, J. G. (1994). MINIMAGE: a program for plotting electron density maps. *J. Appl. Crystallog.* **27**, 649–653.

Braakman, I., Helenius, J. & Helenius, A. (1992). Role of ATP and disulphide bonds during protein folding in the endoplasmic reticulum. *Nature*, **356**, 260–262.

Brennan, M. J., David, J. L., Kenimer, J. G. & Manclark, C. R. (1988). Lectin-like binding of pertussis toxin to a 165-kilodalton Chinese hamster ovary cell glycoprotein. *J. Biol. Chem*. **263**, 4895–4899.

Brünger, A. T. (1992a). *X-PLOR Version 3.1 A system for X-ray Crystallography and NMR*. Yale University Press, New Haven, CT.

Brünger, A. T. (1992b). Free *R* value: a novel statistical quantity for assessing the accuracy of crystal structures. *Nature*, **355**, 472–475.

Burns, D. L. & Manclark, C. R. (1986). Adenine nucleotides promote dissociation of pertussis toxin subunits. *J. Biol. Chem*. **261**, 4324–4327.

Chaudhary, V. K., Jinno, Y., Fitzgerald, D. & Pastan, I. (1990). *Pseudomonas* exotoxin contains a specific sequence at the carboxyl terminus that is required for cytotoxicity. *Proc. Natl Acad. Sci. USA*, **87**, 308–312.

Cini, R. & Marzilli, L. G. (1988). Exploitation of crystalline architecture and solution data in the rational preparation of novel mixed-metal ATP complexes. *Inorg. Chem*. **27**, 1855–1856.

Clairmont, C., Demaio, A. & Hirschberg, C. (1991). Translocation of ATP into the lumen of rat liver and canine pancreas rough endoplasmic reticulum derived vesicles and its binding to lumenal glucose regulated proteins. *J. Cell. Biol.* **115**, 255a.

Donta, S. T., Beristain, S. & Tomicic, T. K. (1993). Inhibition of heat-labile cholera and *Escherichia coli* enterotoxins by brefeldin A. *Infect. Immun.* **61**, 3282–3286.

Freedman, R. B., Hirst, T. R. & Tuite, M. F. (1994). Protein disulphide isomerase: building bridges in protein folding. *Trends Biochem. Sci.* **19**, 331–336.

Galazka, A. (1992). Control of pertussis in the world. *World Health Stat. Quart*. **45**, 238–247.

Gill, D. M. (1978). In *Bacterial Toxins and Cell Membranes* (Jeljaszewica, J. & Wadstrom, T., eds), pp. 291–332, Academic Press, New York.

Gordon, V. M. & Leppla, S. H. (1994). Proteolytic activation of bacterial toxins: role of bacterial and host cell proteases. *Infect. Immun.* **62**, 333–340.

Grant, C. C. R., Messner, R. J. & Cieplak, W., Jr (1994). Role of trypsin-like cleavage at arginine 192 in the enzymatic and cytotonic activities of *Escherichia coli* heat-labile enterotoxin. *Infect. Immun.* **62**, 4270–4278.

Hausman, S. Z. & Burns, D. L. (1992). Interaction of pertussis toxin with cells and model membranes. *J. Biol. Chem*. **267**, 13735–13739.

Hausman, S. Z., Manclark, C. R. & Burns, D. L. (1990). Binding of ATP by pertussis toxin and isolated toxin subunits. *Biochemistry*, **29**, 6128–6131.

Higashi, T. (1989). The processing of diffraction data taken on a screenless Weissenberg camera for macromolecular crystallography. *J. Appl. Crystallog.* **22**, 9–18.

Howson, C. P., Howe, C. J. & Fineberg, H. V. (1991). Editors of *Adverse Effects of Pertussis and Rubella Vaccines*. National Academy Press, Washington.

Jones, T. A., Zou, J.-Y., Cowan, S. W. & Kjeldgaard, M. (1991). Improved methods for building protein models in electron density maps and the location of errors in these models. *Acta Crystallog. sect. A*, **47**, 110–119.

Kaslow, H. R., Lim, L.-K., Moss, J. & Lesikar, D. D. (1987). Structure-activity analysis of the activation of pertussis toxin. *Biochemistry*, **26**, 123–127.

Katada, T. & Ui, M. (1982a). ADP ribosylation of the specific membrane protein of C6 cells by islet-activating protein associated with modification of adenylate cyclase activity. *J. Biol. Chem*. **257**, 7210–7216.

Katada, T. & Ui, M. (1982b). Direct modification of the membrane adenylate cyclase system by islet-activating protein due to ADP-ribosylation of a membrane protein. *Proc. Nat Acad. Sci. USA*, **79**, 3129–3133.

Kraulis, P. (1991). MOLSCRIPT: a program to produce both detailed and schematic plots of protein structures. *J. Appl. Crystallog.* **24**, 946–950.

Krueger, K. M. & Barbieri, J. T. (1993). Molecular characterization of the *in vitro* activation of pertussis toxin by ATP. *J. Biol. Chem*. **268**, 12570–12578.

Krueger, K. M. & Barbieri, J. T. (1994). Assignment of functional domains involved in ADP-ribosylation and B-oligomer binding within the carboxyl terminus of the S1 subunit of pertussis toxin. *Infect. Immun.* **62**, 2071–2078.

Krueger, K. M., Mende-Mueller, L. M. & Barbieri, J. T. (1991). Protease treatment of pertussis toxin identifies the preferential cleavage of the S1 subunit. *J. Biol. Chem*. **266**, 8122–8128.

Laskowski, R. A., MacArthur, M. W., Moss, D. S. & Thornton, J. M. (1993). PROCHECK: a program to check the stereochemical quality of protein structures. *J. Appl. Crystallog.* **26**, 283–291.

Lim, L.-K., Sekura, D. D. & Kaslow, H. R. (1985). Adenine nucleotides directly stimulate pertussis toxin. *J. Biol. Chem*. **260**, 2585–2588.

Madshus, I. G. & Collier, R. J. (1989). Effects of eliminating a disulfide bridge within domain II of *Pseudomonas aeruginosa* exotoxin A. *Infect. Immun.* **57**, 1873–1878.

Mandel, R., Ryser, H. J., Ghani, F., Wu, M. & Peak, D. (1993). Inhibition of a reductive function of the plasma membrane by bacitracin and antibodies against protein disulfide-isomerase. *Proc. Natl Acad. Sci. USA*, **90**, 4112–4116.

Mattera, R., Codina, J., Sekura, R. D. & Bimbaumer, L. (1986). The interaction of nucleotides with pertussis toxin. *J. Biol. Chem*. **261**, 11173–11179.

Merritt, E. A. & Murphy, M. E. P. (1994). Raster3D version 2.0: a program for photorealistic molecular graphics. *Acta Crystallog. sect. D*, **50**, 869–873.

Mortimer, E. A., Jr (1994). Pertussis vaccine. In *Vaccines* (Plotkin, S. A. & Mortimer, E. A., Jr, eds), pp. 91–135, W. B. Saunders Company, Philadelphia.

Moskaug, J. O., Stenmark, H. & Olsnes, S. (1991), Insertion of diphtheria toxin B-fragment into the plasma membrane at low pH: characterization and topology of inserted regions. *J. Biol. Chem*. **266**, 2652–2659.

Moss, J., Stanley, S. J., Burns, D. L., Hsia, J. A., Yost, D. A., Myers, G. A. & Hewlett, E. L. (1983). Activation by thiol of the latent NAD glycohydrolase and ADP-ribosyltransferase activities of *Bordetella pertussis* toxin (islet-activating protein). *J. Biol. Chem*. **258**, 11879–11882.

Moss, J., Stanley, S. J., Watkins, P. A., Burns, D. L., Manclark, C. R., Kaslow, H. R. & Hewlett, E. L. (1986). Stimulation of the thiol-dependent ADP-ribosyltransferase and NAD glycohydrolase activities of *Bordetella pertussis* toxin by adenine nucleotides, phospholipids, and detergents. *Biochemistry*, **25**, 2720–2725.

Munoz, J. J., Arai, H. & Cole, R. L. (1981a). Mouse-protective and histamine-sensitizing activities of pertussigen and fimbrial hemagglutinin from *Bordetella pertussis*. *Infect. Immun.* **32**, 243–250.

Munoz, J. J., Arai, H., Bergman, R. K. & Sadowski, P. L. (1981b). Biological activities of crystalline pertussigen from *Bordetella pertussis*. *Infect. Immun.* **33**, 820–826.

Nambiar, M. P., Oda, T., Chen, C., Kuwazuru, Y. & Wu, H. C. (1993). Involvement of the Golgi region in the intracellular trafficking of cholera toxin. *J. Cell. Physiol.* **154**, 222–228.

Nilsson, T. & Warren, G. (1994). Retention and retrieval in the endoplasmic reticulum and the Golgi apparatus. *Curr. Opin. Cell Biol.* **6**, 517–521.

Ogata, M., Chaudhary, V. K., Pastan, I. & FitzGerald, D. J. (1990). Processing of *Pseudomonas* exotoxin by a cellular protease results in the generation of a 37,000-Da toxin fragment that is translocated to the cytosol. *J. Biol. Chem.* **265**, 20678–20685.

Orlandi, P. A., Curran, P. K. & Fishman, P. H. (1993). Brefeldin A blocks the response of cultured cells to cholera toxin. *J. Biol. Chem.* **268**, 12010–12016.

Pelham, H. R. B., Roberts, L. M. & Lord, J. M. (1992). Toxin entry: how reversible is the secretory pathway? *Trends Cell Biol.* **2**, 183–185.

Read, R. J. (1986). Improved Fourier coefficients for maps using phases from partial structures with errors. *Acta Crystallog. sect. A*, **42**, 140–149.

Sakabe, N. (1991). X-ray diffraction data collection system for modern protein crystallography with a Weissenberg camera and an imaging plate using synchrotron radiation. *Nucl. Instr. Methods, sect. A*, **303**, 448–463.

Sandvig, K. & van Deurs, B. (1994). Endocytosis and intracellular sorting of ricin and shiga toxin. *FEBS Letters*, **346**, 99–102.

Sandvig, K., Ryd, M., Garred, O., Schweda, E., Holm, P. K. & van Deurs, B. (1994). Retrograde transport from the Golgi complex to the ER of both Shiga toxin and the nontoxic Shiga B-fragment is regulated by butyric acid and cAMP. *J. Cell. Biol.* **126**, 53–64.

Stein, P. E., Boodhoo, A., Armstrong, G. D., Heerze, L. D., Cockle, S. A., Klein, M. H. & Read, R. J. (1994a). Structure of a pertussis toxin-sugar complex as a model for receptor binding. *Struct. Biol.* **1**, 591–596.

Stein, P. E., Boodhoo, A., Armstrong, G. D., Cockle, S. A., Klein, M. H. & Read, R. J. (1994b). The crystal structure of pertussis toxin. *Structure*, **2**, 45–57.

Wales, R., Chaddock, J. A., Roberts, L. M. & Lord, J. M. (1992). Addition of an ER retention signal to the ricin A chain increases the cytotoxicity of the holotoxin. *Exp. Cell Res.* **203**, 1–4.

Xu, Y. & Barbieri, J. T. (1995). Pertussis toxin-mediated ADP-ribosylation of target proteins in Chinese hamster ovary cells involves a vesicle trafficking mechanism. *Infect. Immun.* **63**, 825–832.

Yoshida, T., Chen, C., Zhang, M. & Wu, H. C. (1991). Disruption of the Golgi apparatus by brefeldin A inhibits the cytotoxicity of ricin, modeccin, and *Pseudomonas* toxin. *Exp. Cell Res.* **192**, 389–395.

Edited by R. Huber

(Received 4 December 1995; received in revised form 12 February 1996; accepted 16 February 1996)